Surface calibration of electromagnetic properties to simultaneously consider water and chloride contents in concrete both with and without slag

Mohamad Khodor El Achrafi, Géraldine Villain, Stéphanie Bonnet

published in Construction and Building Materials, Elsevier, 417 (2024)
https://doi.org/10.1016/j.conbuildmat.2024.135176

Surface calibration of electromagnetic properties to simultaneously consider water and chloride contents in concrete both with and without slag

Mohamad Khodor El ACHRAFI[1,2], Géraldine VILLAIN[2], Stéphanie BONNET[1]

[1] Nantes University, Ecole Centrale Nantes, CNRS, GeM, UMR 6183 F-44600 Saint-Nazaire France
mohamad.el-achrafi@univ-nantes.fr, stephanie.bonnet@univ-nantes.fr
[2] Univ Gustave Eiffel, MAST-LAMES, Campus de Nantes, Allée des Ponts et Chaussées, CS5004, F-44344 Bouguenais, France
geraldine.villain@univ-eiffel.fr

Abstract: **In this work, novel calibration curves and calibration surfaces of Electromagnetic (EM) characteristics are modeled as a function of the water and chloride contents of concrete. An experimental campaign was carried out on cores extracted from two types of concretes: C1 (Ordinary Portland Concrete) and C3 (62% slag + 38% clinker). The cores were initially saturated at three sodium chloride (NaCl) concentrations and then oven-dried to attain different degrees of saturation. They were tested with the electromagnetic and electrical cell to determine the dielectric permittivity and electrical resistivity, respectively, at the targeted hydric and chloride ion contents. The calibration curves and calibration surfaces, which represent the resistivity and permittivity as a function of chloride content and/or degree of saturation, were adjusted and presented for both concretes. The calibration surfaces developed herein serve as an essential tool to study complex phenomena, such as the coupled water-chloride ingress.**

Keywords: electrical resistivity, dielectric permittivity, chloride content, degree of saturation, non-destructive testing (NDT).

1. Introduction

Non-destructive testing (NDT) methods based on the propagation of electromagnetic waves are increasingly being used to study and assess the durability of reinforced concrete (RC) structures in marine environments [1–4]. This paper focuses on the existing NDT methods applied to measure electrical resistivity (ρ) and dielectric permittivity (ε). These two EM characteristics have in fact been selected due to their sensitivity to the water and chloride content of concrete [5–11]. The significant presence of chloride in the concrete pore solution increases its electrical conductivity and leads to lower bulk resistivity [12,13]. However, several studies have found that the impact of chloride on the bulk resistivity of concrete is much less apparent than that of the degree of concrete saturation [14,15]. The majority of studies reveal a significant power-law dependency of concrete resistivity and degree of saturation, which has been expanded from Archie's Law [16] and applied to concrete with satisfactory results.

Moreover, only a limited investigation has been carried out on the nature of the relationship between concrete permittivity and chloride or water content. As a result of interfacial polarization, which entails a complicated phenomenon known as the Maxwell-Wagner effect [17], the EM response is highly frequency-dependent for concrete that contains an ion-rich pore solution. Under saturated conditions, the permittivity of chloride-contaminated concrete is significantly higher at low radar frequencies (0.1-0.4 GHz), as compared to uncontaminated concrete, while remaining similar at high radar frequencies (1-1.5 GHz) [18]. However, under dry conditions, the relative permittivity seems to be practically non-dispersive with respect to the frequency range, with a very slight effect from the chlorides, which have been crystallized in the pores [18]. Laurens *et al.* [19] asserted that the permittivity remains frequency-independent for dry concrete (with solid and gaseous phases only). Thus, dispersion in concrete arises solely from the presence of water in the pores, and moreover its impact is determined by the volume of water content. Accordingly, a strong linear relationship exists between the degree of saturation and the permittivity [20,21]. For radar frequencies ranging from 0.1 to 3 GHz, the dielectric constant of the solid components of concrete varies between 3 and 8 while that of water is significantly higher (≈ 81) [22]. Therefore, the concrete permittivity values are greater at higher degrees of saturation. Although, it is possible to measure the permittivity of dry concrete, determining its resistivity is not feasible when the degree of saturation falls below 35-40%, depending on the concrete mix design [10].

In addition, several methods to assess the presence of chloride have been analyzed, yet few can quantify the chloride content, which happens to be the purpose herein [23]. Let's note the promising methods being developed, such as electrical impedance spectroscopy [24], which however remains difficult to use *in situ*.

Experimental calibration laws between the resistivity or permittivity and the degree of saturation (S_r) or chloride content (C) of the concrete can establish this sensitivity [21,25–28,11]. Such calibration laws are usually introduced independently to convert the resistivity (ρ) profile into a degree of saturation (S_r) profile [29,30] or a chloride content (C) profile [11,31] or, in a similar way, the permittivity (ε) profile into a degree of saturation (S_r) profile [32] or a chloride content (C) profile [4]. During an imbibition test with freshwater (i.e. without salt), the permittivity and resistivity of concrete depend solely on the water content in concrete and the ions present in the pore solution [29,32–36].

Moreover, during a chloride diffusion test, these two physical characteristics depend solely on the chloride content since the concrete is completely saturated [2,6,31,37,38,11]. Thus, these

experimental conditions justify that the research undertaken has studied the evolution of these characteristics with chlorides or water content independently.

However, RC structures in a marine environment, i.e. in tidal zones, are submitted to drying and wetting cycles, thus resulting in varying degrees of saturation in the cover concrete, whereas chloride penetrates with the liquid phase by convection as well as by diffusion [39–42]. Thus, the variations in the resistivity (ρ) and permittivity (ε) are due to the simultaneous chloride and water content variations. It is therefore essential to determine the calibration surface that links the concrete permittivity or resistivity to the water and chloride content.

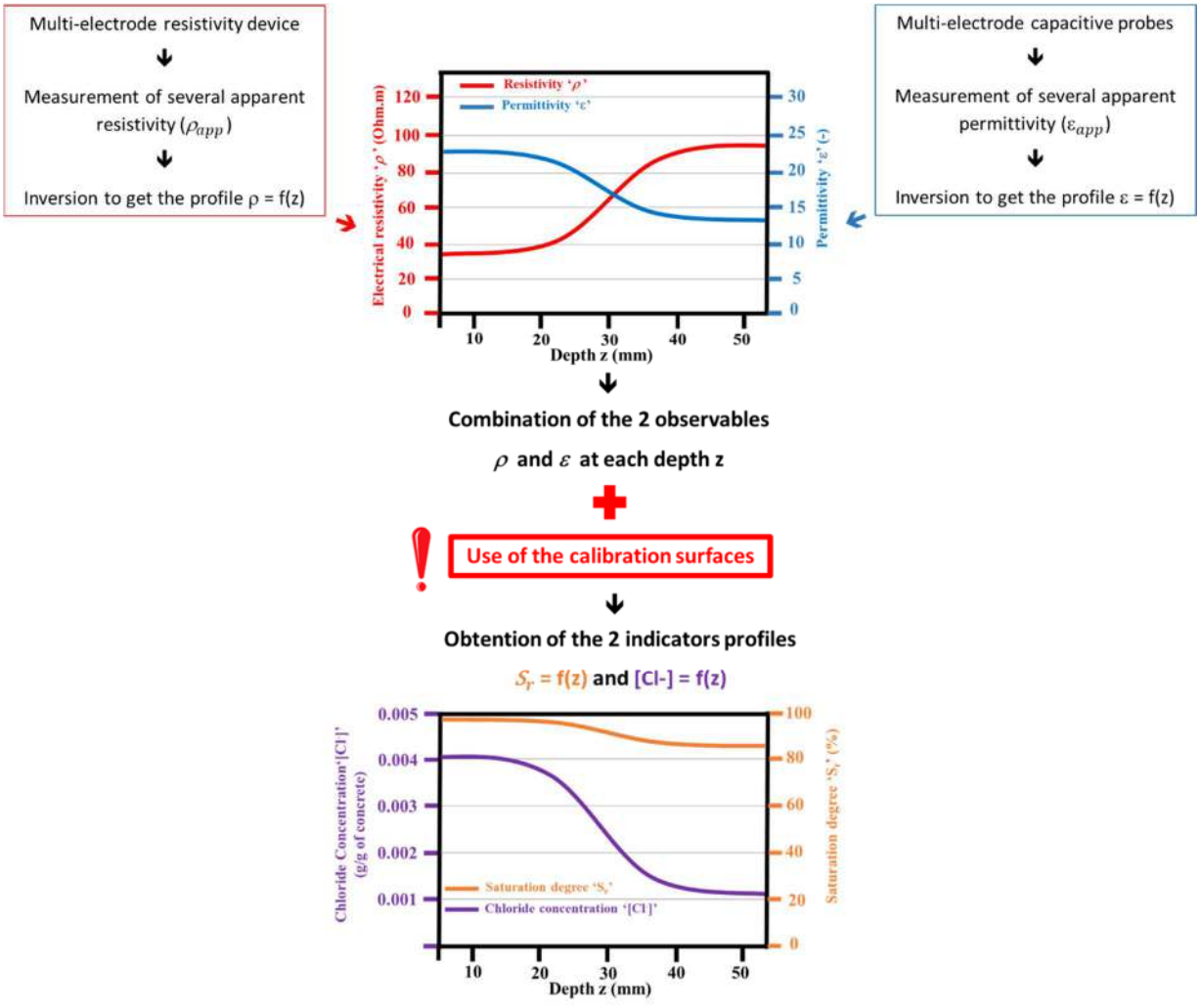

Figure 1: Methodology for an *in situ* structural assessment using calibration surfaces

For real marine structures, the cover concrete displays heterogeneous values of degree of saturation and chloride content, which lead to different values of resistivity (ρ) and permittivity (ε). Thus, for an on-site survey, the inspector must first determine both the resistivity and permittivity profiles by inverting the apparent resistivity (ρ_{app}) and apparent

permittivity (ε_{app}) obtained by the multi-electrode resistivity device [11,30,31] and multi-electrode capacitive probes [30,32], respectively, as depicted in Figure 1. The inspector then converts the NDT observables into both the indicator profiles (degree of saturation and chloride content) by combining the two NDT observables at each depth (z) and by using the calibration surfaces. Thus, it becomes mandatory to dispose of the system of equations linking the observables to the two unknown indicators and define the calibration surface as explained for the bulk evaluation of concrete indicators in [4], in order to evaluate the indicator profiles.

The aim of this paper therefore is to build these calibration curves and calibration surfaces for resistivity and permittivity as a function of both free and total chloride content. For this purpose, we carried out a complete experimental campaign based on non-destructive (ND) and destructive (D) testing to determine (S_r) as well as free and total chloride content in two representative concrete mixes with and without slag, given that slag is particularly used for RC structures in marine environments [43,44]. In addition, we aim to investigate the influence of slag incorporation on the electromagnetic (EM) characteristics of concrete. The chloride-binding influence will be studied as well. It is well-known that the electrical current and polarization phenomena primarily occur by means of ions dissolved in the pore solution [14,6]. Therefore, understanding the impact of chloride binding becomes crucial.

The procedure adopted to carry out this work is summarized as follow. First, concrete cores are initially saturated with three different sodium chloride (NaCl) concentrations, then oven-dried to reach various degrees of saturation. Second, the cores are tested with the electromagnetic and electrical cell to determine the permittivity and resistivity, respectively, at the targeted hydric and chloride ion contents. Third, calibration curves and calibration surfaces are modeled by fitting the experimental measurements.

This paper has been divided into 5 sections. An overview of the studied concretes, measurement methods and experimental protocol is presented in Section 2. While section 3 describes the calibration curves and then the calibration surfaces. These results are discussed in Section 4 and a conclusion is offered in Section 5.

2. Materials, measurement methods and experimental protocol

2.1. Materials

Two concrete mixes are studied in this work (see Table 1), one with slag (C3) the other without (C1). The mixes are quite similar for both concretes, except the type of binder. The binder of concrete C1 is an ordinary Portland cement CEM I 52.5 N CE CP2 NF while that of

concrete C3 is composed of 16% calcareous filler addition and 84% CEM III/A 52.5 L PMES CP1 NF. The cement CEM III/A, containing at least 60% CEM, is widely used for structures in marine environments [43–45]. Both concretes were mixed in a concrete plant, in the aim of achieving the same resistance and same porosity for C1 and C3. For this reason, the mix design was adapted by adding a calcareous filler to replace a portion of the CEM III. Moreover, the mineral origin changes: the sand 0/2 is crushed from gneiss, the sand 0/4 is alluvial, i.e. rolled in the river, and the crushed aggregates are amphibolite (6/10) and corneal (11/22).

The concretes studied in this work were cast and demolded in 2013. The concrete slabs were completely immersed in tap water after casting until the beginning of the experimental campaign in January 2020.

For the calibration campaign, six cores (d = 75 mm, h = 70 mm) were extracted from one slab of each concrete. The dimensions respect the representative elementary volume (REV) of the concrete. Sodium hydroxide was dissolved in the freshwater to maintain a pH of 13, so as to prevent leaching. The freshwater was replaced every two years. Since the pH verification was not checked frequently, a risk of leaching arose; hence, two experimental steps were performed to avoid this bias: 1) the calibration cores were initially extracted from the center of slabs with a total thickness of 13 cm; and 2) 3 cm were subsequently cut from each core surface to remove any carbonated or leached portion of the concrete due to the long curing time.

The durability indicators determined at 6 years of curing for both concretes were given in the findings by El Achrafi et al., [11]. Nevertheless, the porosity accessible to water ϕ (%) obtained at 6 years will be the only durability indicator presented in this work (Table 1); it was measured for three cores (d = 70 mm; h = 25 mm) of each concrete by means of hydrostatic weighing [46]. The average and standard deviation values are displayed in Table 1.

Table 1: Mix designs of the studied concretes

Constituents (kg/m^3 of concrete)	**Concrete C1**	**Concrete C3**
Aggregate (6/10)	320	320

Aggregate (11/22)	760	760
Sand (0/2)	560	430
Sand (0/4)	300	430
CEM I 52,5 N CE CP2 NF	305	-
CEM III/A 52.5 L PMES CP1 NF	-	260
Calcareous filler addition	-	50
Sika Prise SC2	0.7	-
SikaPlast Techno 80	-	1.9
Effective water	190	177
Water-to-cement ratio (w/c)	0.62	0.68
Water-to-binder ratio (w/b)	0.62	0.58
Porosity ϕ (%) at 6 years	16.82 ± 0.2	15.89 ± 0.14

2.2. NDT measurement methods: Resistivity and coaxial cells

The electrical resistivity measurements were performed using the resistivity cell developed by Du Plooy *et al.*, [47]; this cell was connected to a resistivity meter (Syscal Pro 96, IRIS Instruments) that made it possible to both control the generation of electric current and record the signals from the various electrodes (Figure 2.a). The potential drop between two electrodes was measured at five different heights using an alternating current applied to the two exterior surfaces, with two measurements being conducted at the highest height (ΔV_1). Two sets of measurements recorded the resistivity in the two directions of the core, as described in Figure 2.a; the total number of measurements was 12 per core. The average of the 12 measurements and the standard deviation were calculated for each core.

The dielectric permittivity (ε) measurements were conducted using the cylindrical coaxial electromagnetic cell developed by Adous *et al.,* (2006) [48]. This technique is among those employed to characterize the complex dielectric permittivity of hydraulic concrete over a wide frequency band (50 MHz to 1.6 MHz). The device consists of a cylindrical-coaxial transmission line, on which a vectorial network analyzer is connected to the cell by a coaxial cable, as well as a sample holder, and a computer connected to the analyzer (Figure 2.b). The underlying principle is to measure the reflection coefficient of the EM wave in the tested sample, which depends on the both sample geometry and the material permittivity. An iterative inversion method retrieves the complex dielectric permittivity from the reflection coefficient measurements, then the dispersion curve of the complex permittivity is obtained. The extracted permittivity is the real part of the relative complex permittivity at low frequency equal to 33 MHz since permittivity is more sensitive to chloride ions at low frequency [6,18,49].

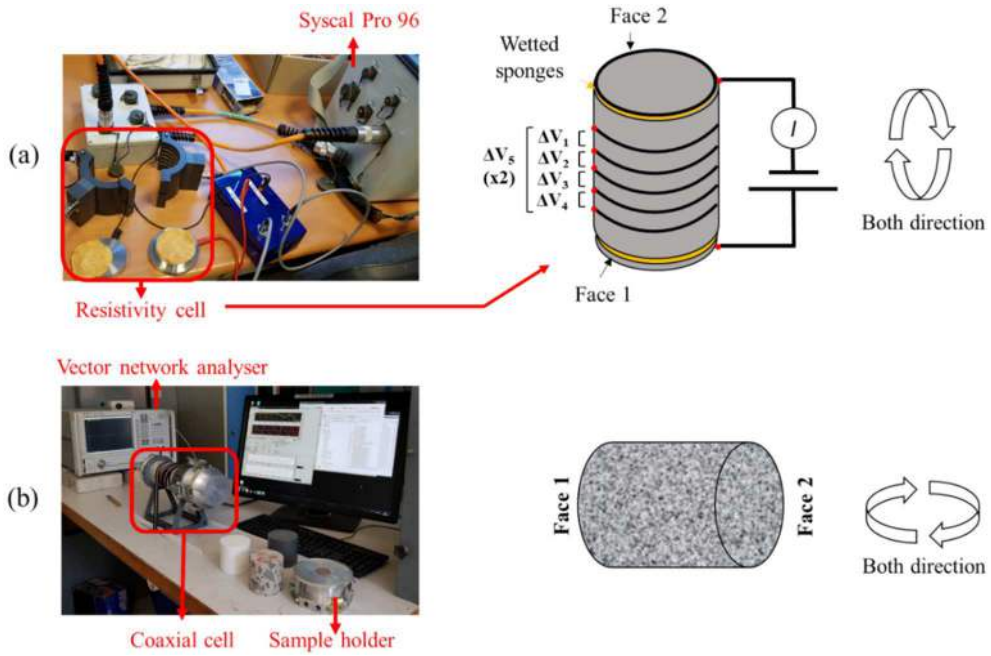

Figure 2: Measurement devices: a) resistivity cell, b) coaxial cell

2.3. Destructive measurement methods

A destructive measurement was carried out at the end of ND testing to determine the real degree of saturation (%) of the cores and the real free and total chloride contents in the cores. The destructive measurement method will be presented in the following subsection.

2.3.1.The real degree of saturation S_r (%)

As mentioned above, the porosity accessible to water ϕ (%) was measured for three cores (d = 70 mm; h=25 mm) of both concretes by means of hydrostatic weighing [46]. Keep in mind that these samples are distinct from the calibration samples. In accordance with this method, the cores were subjected to a destructive test by being exposed to an oven-drying process at 105°C.

The mass of the calibration cores $m_{(t)}$ (g), corresponding to the targeted degree of saturation S_r (%) outlined in Table 2, was determined using Eq. 1, where m_{sat} (g) and m_w (g) represent the mass of the saturated cores ($S_r = 100$ %) and the mass of water in the saturated cores obtained by Eq. 2, respectively. The volume of the calibration cores V (cm^3) was determined by means of hydrostatic weighing [46]. This approach was adopted in considering that the cores used to determine porosity had been extracted from the same slab as the calibration cores, thus ensuring similar porosity characteristics across all samples.

$$S_r = \frac{m_t - (m_{sat} - m_w)}{m_w}.100 \quad \text{Eq. 1}$$

$$m_w = V.\frac{\phi}{100} \quad \text{Eq. 2}$$

2.3.2. Concentration of free and total chloride (g of chloride/g of concrete)

In order to determine the concentration of free (C_f) and total (C_t) chloride, a destructive measurement was performed. The chloride concentration was derived using the following experimental protocol, as depicted in Figure 3.

In step 1, the cores were sawn into three parts: (1) from 0 to 25 mm, (2) from 25 to 50 mm, and (3) from 50 to 70 mm. Next in step 2, each part was ground, with vibrating disc mill RS200® to obtain a powder with 20 µm of fineness. Step 3 involved extracting water-soluble ions (including free chloride ions) and total chloride ions based on the procedure recommended by the RILEM Association [50,51]. Step 4 of the protocol relied on potentiometric titration to determine the free and total chloride concentrations. The average of the three chloride concentrations was then calculated to determine the free and total chloride contents of each core.

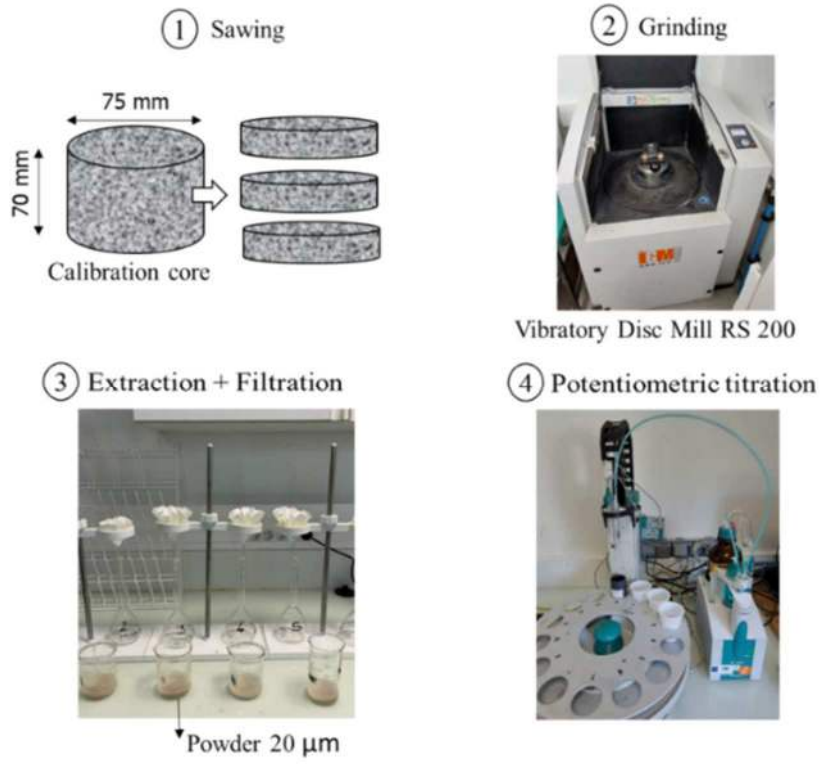

Figure 3: Experimental protocol to determine the free and total chloride contents in the cores

2.4. Experimental protocol and measurements

The experimental protocol followed in this work is based on the work by Villain *et al.*, (2018) [28] to generate the calibration curves as a function of the degree of saturation; this step was adapted by Fares *et al.,* (2018) [11,31] to derive these curves as a function of the free chloride content. Figure 4 illustrates all the steps of the experimental protocol undertaken to obtain both the calibration curves and calibration surfaces.

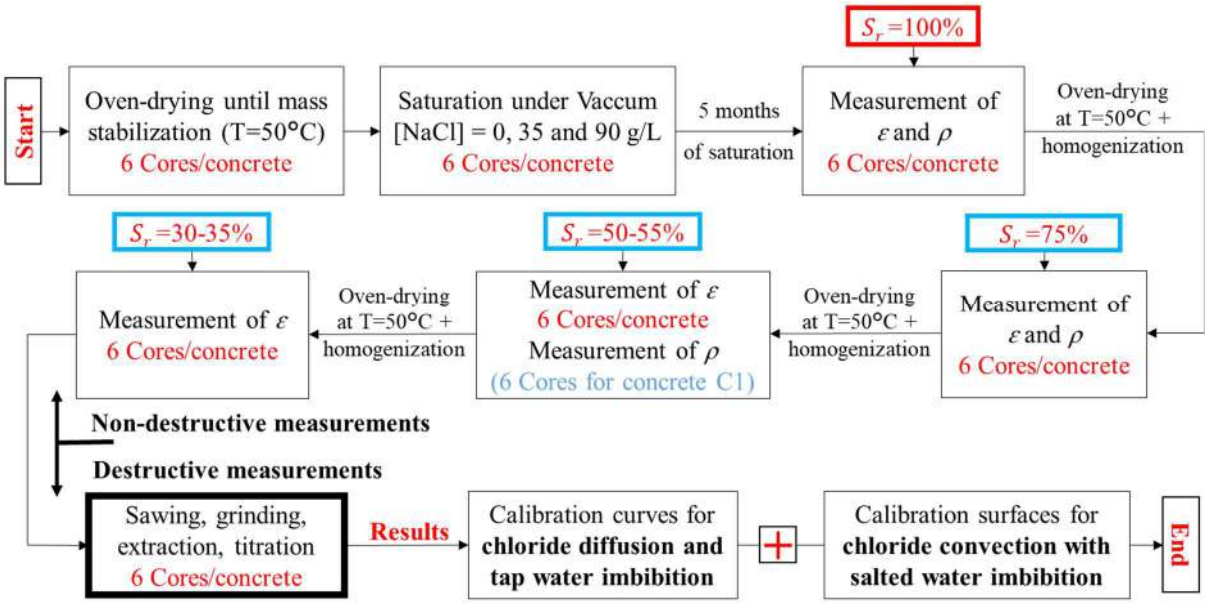

Figure 4: Experimental protocol to determine the calibration curves and calibration surfaces

At first, the cores were oven-dried at 50 °C until their masses stabilized. The drying period was 4 and 9 weeks for concretes C1 and C3, respectively. The cores were then saturated under vacuum with three different sodium chloride concentrations [NaCl] = 0, 35 and 90 g/L (2 cores per concentration) given that similar concentrations can be found in seawater [52] or deicing products. Table 2 presents the core conditioning specifications associated with the different ionic and hydric states for both concretes.

The resistivity and permittivity of the cores were then measured after 5 months of immersion in the salt solution in order to attain the chloride equilibrium fixation [53,54], after which the cores were oven-dried at T = 50°C to reach various masses and therefore various degrees of saturation (S_r = 75%, 50-55% and 30-35%), as per the procedure described in Section 2.3.1. The degrees of saturation obtained differ slightly from the targeted values since it was impossible to weigh the cores when the laboratory was closure.

Table 2 : Calibration core conditioning

Nomenclature	Concrete	[NaCl] + [NaOH]		Targeted S_r(%)			
				100%	75%	50-55%	30-35%
C1-1-0	C1	0 g/L of NaCl + 4 g/L of NaOH	Obtained S_r (%)	100	72.75	45.83	28.23
C1-2-0				100	76.23	-	31.24
C3-1-0	C3			100	76.26	48.61	26.62
C3-2-0				100	75.88	-	26.06
C1-1-35	C1	35 g/L of NaCl + 4 g/L of NaOH		100	74.72	57.00	32.88
C1-2-35				100	76.93	57.71	36.52
C3-1-35	C3			100	73.81	59.29	37.42
C3-2-35				100	76.49	59.93	35.66
C1-1-90	C1	90 g/L of NaCl + 4 g/L of NaOH		100	76.38	58.73	35.01
C1-2-90				100	78.35	57.79	37.53
C3-1-90	C3			100	76.20	59.62	36.02
C3-2-90				100	77.54	59.67	35.49

In order to homogenize the cores (i.e. equal water content along the depth profile) at each degree of saturation reached, the cores were sealed with an adhesive aluminum foil and then they were placed back in the oven at T = 50°C for an additional amount of time. The duration of this additional period matched the time required for oven-drying to achieve the desired degree of saturation [55]. The cores were removed again from the oven to reach ambient temperature. Subsequently, they were unsealed, and permittivity and resistivity measurements were conducted.

Once all the electrical resistivity and dielectric permittivity measurements (ND) had been carried out, the destructive measurements presented in Section 2.3.2 were performed to identify the real chloride concentrations in each core.

The **calibration curves and calibration surfaces** were produced to express resistivity or permittivity as a function of free and/or total chloride concentration and/or as a function of saturation degree.

3. Results and Discussion

In this section, the calibration curves representing resistivity and permittivity versus degree of saturation will be presented first and versus chloride content thereafter. Next, the calibration surfaces representing resistivity and permittivity versus chloride content and degree of saturation will be provided. The results obtained for concrete C1 are displayed in blue while those obtained for concrete C3 are in green.

3.1. Calibration curves

3.1.1. Resistivity and permittivity versus degree of saturation (NaCl=0 g/L)

The calibration curves relating resistivity and permittivity with the degree of saturation shown in Figure 5 were obtained by fitting the results with a power and linear function, respectively. The results presented are those obtained for cores saturated with tap water without chloride (C1-1-0, C1-2-0, C3-1-0, C3-2-0). It is common to use logarithmic values since concrete resistivity has several orders of magnitude due to its high sensitivity to water and chloride content [16,56,57]. However, the calibration curves were also presented with non-logarithmic values to show the strong influence of water and chloride content. The regression coefficients derived are not lower than 0.96 for both concretes. Let's note that the resistivity decreases with an increase in the degree of saturation (S_r) while permittivity increases. These results are similar to those obtained in the literature review with different coefficients given that the concrete mixtures differ [7,13,37,58].

Moreover, it was impossible to determine the concrete resistivity at various partially saturated states, i.e. at $S_r < 35\%$ for concrete C1 and at $S_r < 75\%$ for concrete C3. The contact resistance was very high; therefore, the injected tension had to be substantial. Thus, the Syscal fails to measure the intensity of the current or potential drop. It was also possible that electric current could not circulate into the concrete because the liquid phase is discontinuous in porous media. These findings confirm those reported by Polder and Henry [14,15], who demonstrated the significant impact of water content on concrete electrical resistivity. Consequently, the resistivity calibration curves for concrete C3 were established using just two measurements for two different degrees of saturation (S_r = 100 and 75%), which raises questions about the reliability of the calibration equation coefficients.

On the other hand, let's remark that the resistivity of concrete C3 is 10 times higher than that of concrete C1 for S_r=100%. This finding can be explained by both the consumption of

hydroxyl ions during the latent hydraulic reaction of slag [59–62] and the formation of new C-S-H hydrate gel, which densifies of the microstructure and decreases the pore solution volume [63,64]. This greater resistivity exhibited by C3 could explain why the degrees of saturation at which resistivity measurements become infeasible are higher for C3 (S_r < 75%) than for C1 (S_r < 45 %).

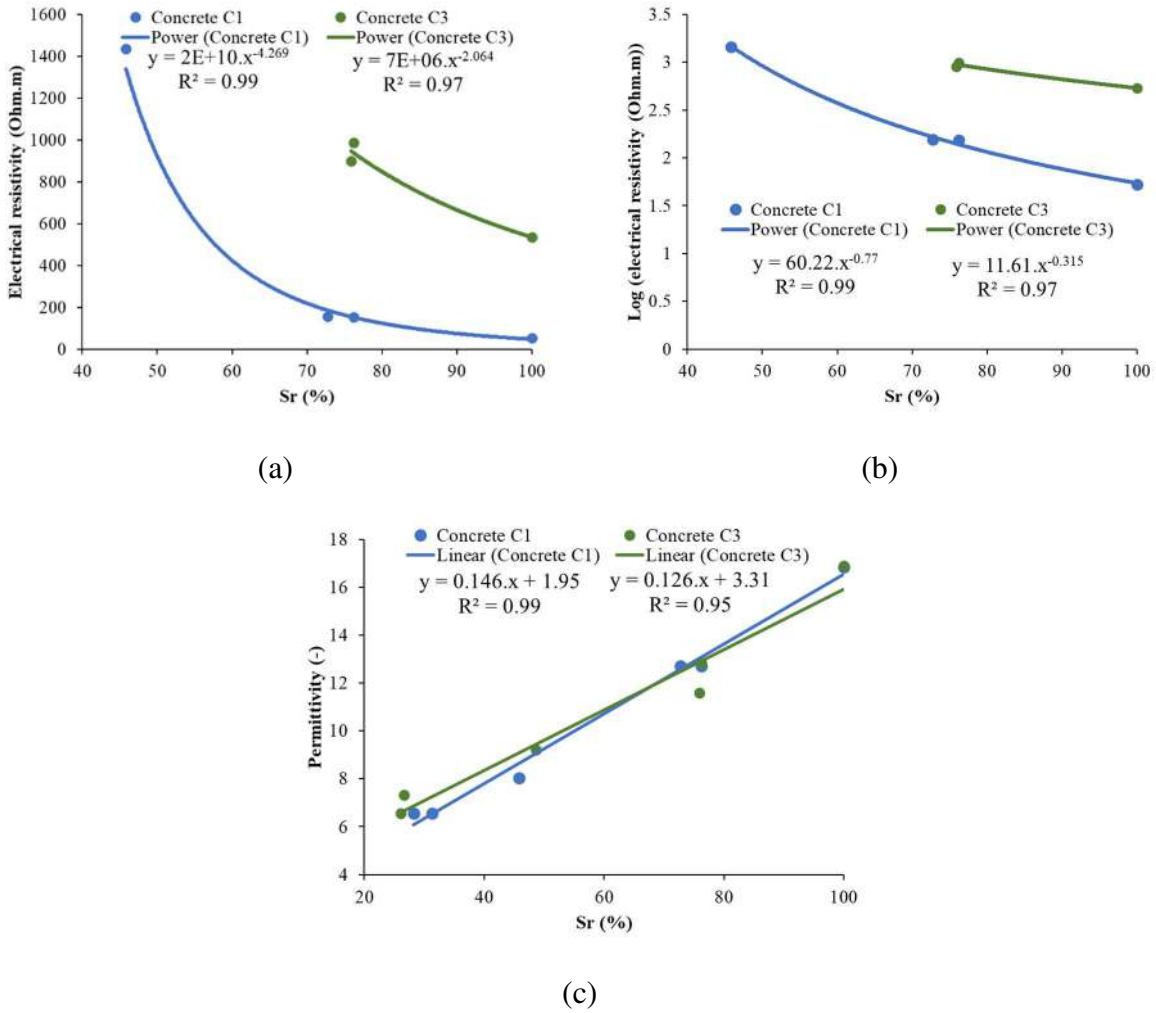

Figure 5: a) resistivity, b) Log resistivity, and c) permittivity vs. concrete degree of saturation (S_r)

As regards the permittivity results, the coefficients of the calibration equation obtained for both concretes exhibit a slight difference compared to the values reported in the literature for highly similar concretes [4,34]. In contrast with the increase in electrical resistivity observed when substituting Portland cement with slag, the permittivity measurements exhibit similar values for both concretes, regardless of the degree of saturation. However, it was to be expected that the permittivity of C3 would be lower than that of C1. Indeed, the permittivity of a medium submitted to an electrical field is related to the phenomenon of polarization due

to the local redistribution of 'fixed' charges, whereas resistivity is more closely related to the conduction phenomenon due to the movement of 'free' charges [65]. One of the main, yet not unique, effects of slag on the number of free charges is the consumption of hydroxyl ions (OH^-) in the interstitial solution. Thus, the effect of slag will be more pronounced on the electrical resistivity than on the dielectric permittivity. Moreover, permittivity seems rather insensitive to the difference in hydrates formed in these two cementitious matrices.

In addition, the results presented by Chen et al., [34] show similar permittivity values to those obtained in this study for fresh concrete both with and without slag, using ground-penetrating radar (GPR) at the significantly higher frequency of 1.5 GHz.

Chen *et al.,* (2012) [34] also suggested that slag has a negligible effect on permittivity for a totally saturated concrete. However, our findings indicate similar permittivity values for both concretes C1 and C3, regardless of the degree of saturation, which serves to refute Chen's hypothesis regarding the volumetric effect of water on these values.

3.1.2.Resistivity and permittivity versus chloride concentration (S_r=100 %)

Before presenting the calibration curves that express resistivity or permittivity as a function of chloride content, let's present the real chloride concentrations of the calibration cores obtained through DE for both concretes (see Figure 6). Since the cores had been cut into three parts, three values of total and free chloride concentrations are shown in the middle of each part. The average of these three values is used in the calibration curves vs. measured resistivity or permittivity. As for the two cores without chlorides, the chloride concentration was determined for only one core per concrete (C1-2-0 and C3-2-0).

These results show good uniformity in chloride concentration, except for core C1-90-6, which exhibits higher concentrations at the ends than in the middle. Indeed, we observed a higher proportion of aggregates compared to the cement matrix in the middle part of core C1-90-6. This disparity can potentially significantly influence the distribution of chlorides in the core, since chlorides primarily penetrate through the cement paste rather than into the aggregate matrix.

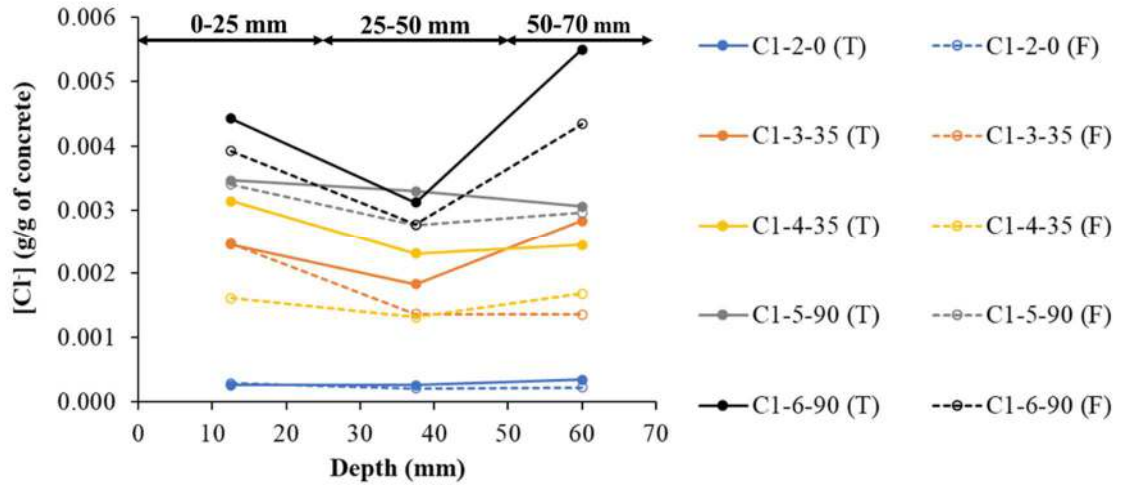

(a)

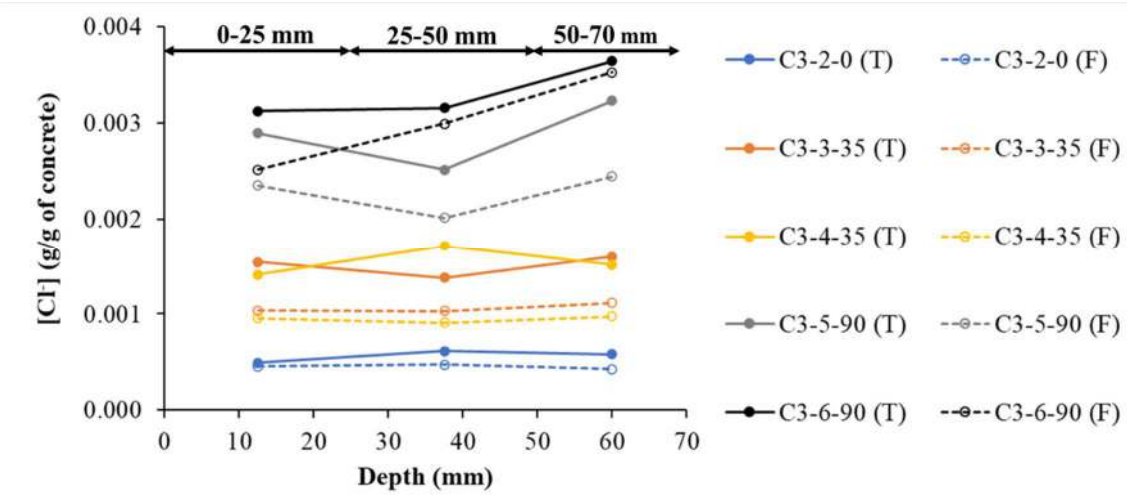

(b)

Figure 6: Concentrations of free and total chlorides in the calibration cores: (a) C1, (b) C3

Moreover, the resistivity measurements (ΔV_1 to ΔV_5) recorded for the chloride-contaminated calibration cores under saturated conditions ($\boldsymbol{S_r}$=100 %) are depicted in Figure 7. Since resistivity measurements were carried out in both directions within the cores (Figure 2.a), results are presented for directions (1) and (2) using dashed and continuous lines, respectively. These results reveal a consistently uniform resistivity measurement along the cores, which can be ascribed to the uniform chloride distribution, as illustrated in Figure 6. For core C1-6-90, a notable increase in resistivity is found for measurements ΔV_3 and ΔV_4, both located in the core's middle section. This increase in resistivity is directly correlated with the lower chloride concentration data obtained in this part of the core, as shown in Figure 6.a.

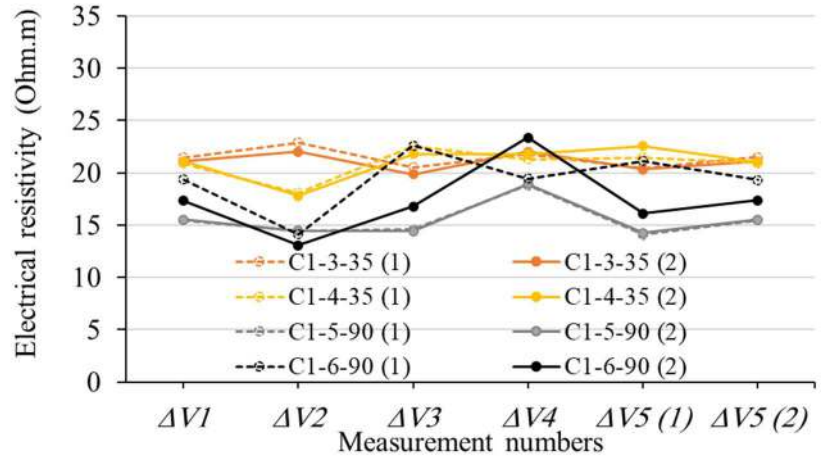

(a)

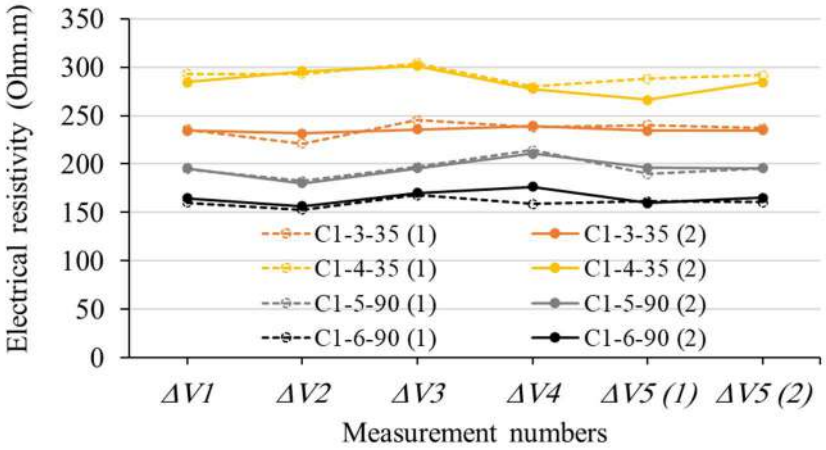

(b)

Figure 7: Resistivity measurements obtained at different positions along the chloride-contaminated cores under saturated conditions (S_r=100 %) for both concretes: (a) C1, (b) C3

The resistivity and permittivity calibration curves versus free and total chloride concentrations are presented in Figure 8 and Figure 9, respectively. The resistivity curves versus chloride content have also been drawn with and without logarithmic resistivity values like those versus the degree of saturation. Moreover, the calibration curves versus *total* chlorides are indicated with a solid line and the curves vs. *free* chlorides with a dashed line. Let's point out that the resistivity and permittivity results presented in this section have been obtained for completely saturated cores (S_r=100 %).

The resistivity results in Figure 8 show a significant decrease in resistivity for both concretes with an increase in chloride concentration. The elevated conductivity of chloride ions present in the pore solution results in a reduction of the resistivity of the pore solution, consequently

leading to a decrease in the bulk resistivity of the concrete. These results are similar to those obtained in the literature for ordinary Portland concretes [6,37,59].

The calibration curves were generated by fitting the results using a power function with a regression coefficient not lower than 0.93 for both concretes. In addition, results show that the resistivity is more sensitive to an increase at lower NaCl concentrations of the pore solution (0 g/L < [NaCl] < 35 g/L) but less so at higher concentrations ([NaCl] = 90 g/L). These results are similar to those obtained by Sbartai *et al.,* [13], who noted with the more acute steepness of the calibration curve between 0 and 35 g/L of NaCl compared to that between 35 and 90 g/L.

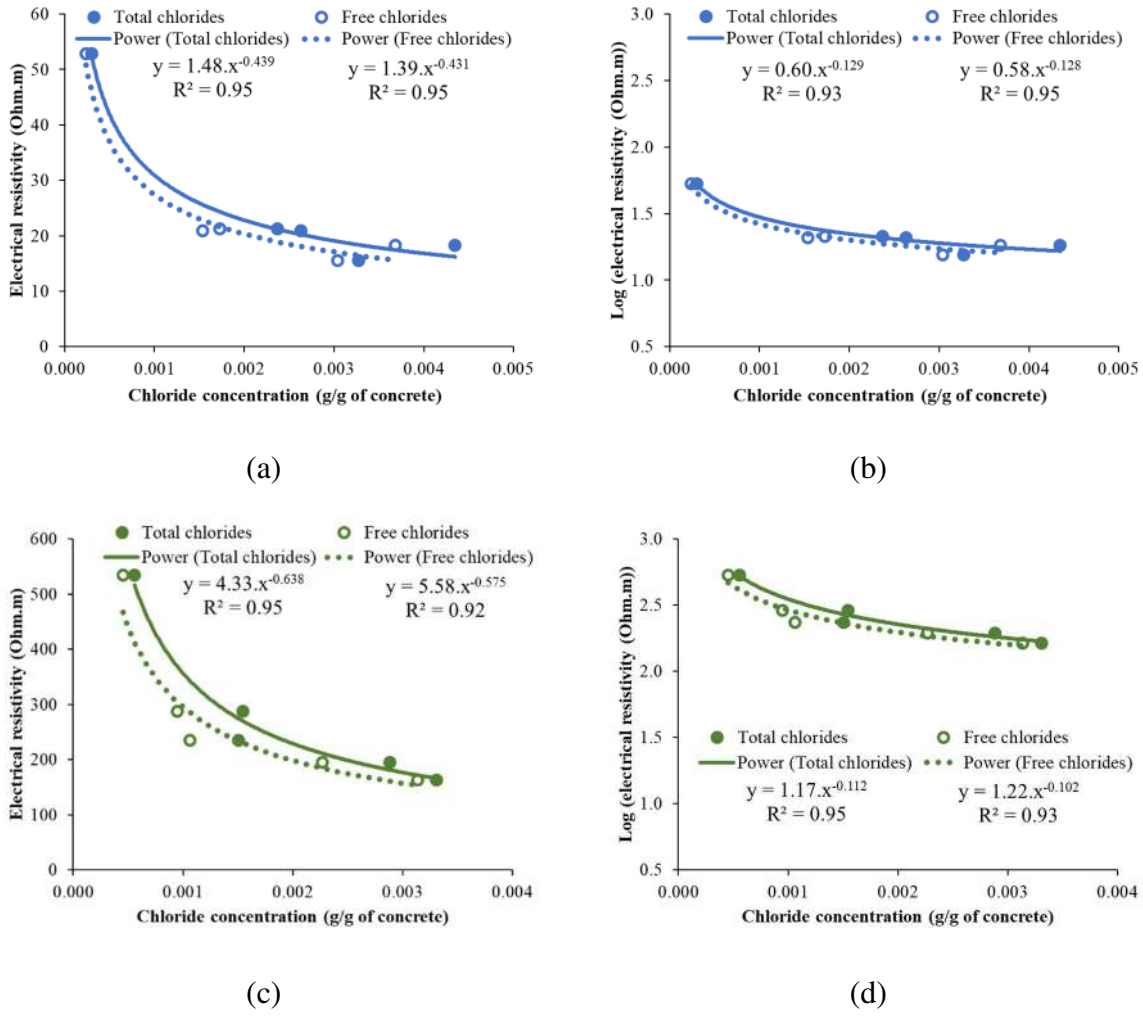

Figure 8: Resistivity versus free and total chloride concentration: (a,b) concrete C1, (c,d) concrete C3 (S_r=100 %)

Based on these experimental findings, it was observed that a transition in degree of saturation from 100% to 35% resulted in a substantial (90%) reduction in the resistivity of concrete C1. In comparison, an increase in sodium chloride (NaCl) concentration from 0 g/L to 90 g/L led

to a comparatively lower 61% decrease in resistivity. These results underscore the greater impact of degree of saturation on concrete resistivity, outweighing the influence of chloride content. Moreover, they align with the findings obtained by Polder [14] and Henri [15].

As for the permittivity results, these novel calibration curves had not been previously investigated, especially for concretes with slag, e.g. C3. The calibration curves presented in Figure 9 were fitted with a linear model whose regression coefficients were not lower than 0.95 and 0.58 for concretes C1 and C3, respectively. The reduced value of the regression coefficient for concrete C3 can be attributed to the low permittivity value observed for core C3-90-5. When excluding this core from the analysis, the regression coefficient improved to 0.92 and 0.8 for the total and free chloride calibration curves, respectively. Before conducting the measurements, the external surface of the cores was wiped to reduce the impact of excess water; however, it appears that core C3-90-5 was excessively wiped, causing partial drying and resulting in a lower permittivity value.

Furthermore, these findings reveal that concrete C3 exhibits lower permittivity than concrete C1 despite both having the same-targeted concentrations of NaCl. It is to be noted however that the real chloride concentrations obtained through destructive measurements are higher for concrete C1 than for C3, which explains the lower permittivity values observed for C3. This low chloride content within the cores of concrete C3 can be attributed to the low chloride diffusivity and the refinement of the microstructure of this concrete due to slag [11,62,63,66].

Regardless of the chloride content in both concretes, it can be remarked that the permittivity of concrete C3 exhibits less sensitivity to chloride content compared to C1. As an example, at the same chloride concentration of 0.003 g/g of concrete, the results reveal permittivity values of 32 for concrete C1 and 24 for concrete C3 (as indicated by the red arrows in Figure 9). This feature, which is difficult to explain, could be due to a lower redistribution of the fixed charges for concrete C3 at the interface between the cementitious matrix and the pore solution contaminated with chlorides.

Figure 5.c shows the same trend in calibration curves for both concretes versus degree of saturation. Hence, we can deduce that permittivity is more closely correlated with the ion content present in its pore solution than its water content.

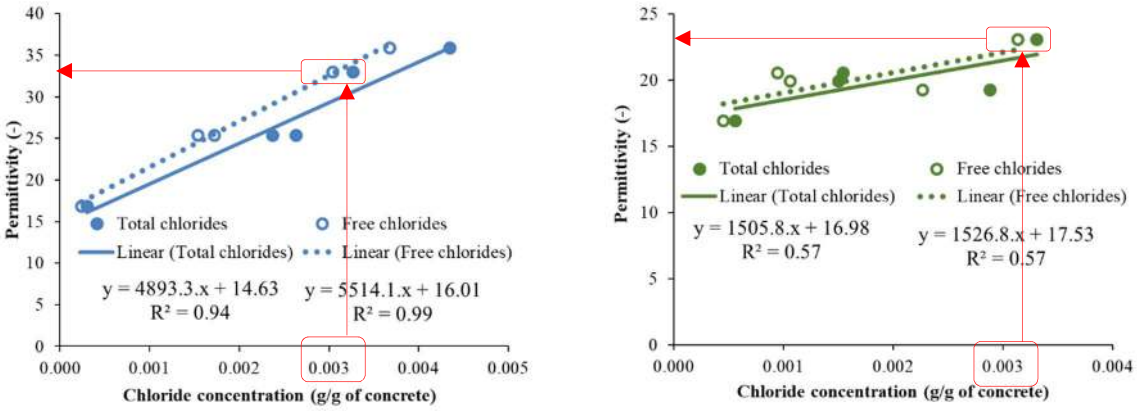

(a) ;(b)

Figure 9: Permittivity versus chloride concentration: (a) concrete C1, (b) concrete C3 (S_r=100 %)

3.2. Calibration surfaces

All experimental measurements were first presented as filled points in 3D graphs where the x-axis represents the total or free chloride concentration, the y-axis the degree of saturation, and the z-axis the permittivity or the resistivity measured at a known chloride concentration and degree of saturation.

The calibration surfaces were modeled by fitting the experimental results with a polynomial function, using Eq. 3 for resistivity and Eq. 4 for permittivity, where 'C' (g/g of concrete) and 'S_r' (%) represent the chloride concentration and degree of saturation of concrete, respectively. The curve fitting toolbox on MATLAB® software served to model these surfaces.

As a first step, the fitting was carried out with a polynomial equation of different degrees. The degrees of the polynomials were chosen so as to obtain the highest regression coefficient R^2 (not less than 0.90) in order to achieve the best fit. The use of logarithmic resistivity values led to removing the quadratic effect and deriving a polynomial equation of degree one with respect to x-axis and y-axis (see Eq. 3).

Nevertheless, fitting the permittivity surface according to a polynomial equation of degree one with respect to the x and y axes has led to a regression coefficient R^2 less than 0.9 (≈0.87), especially for concrete C3. The low regression coefficient values obtained from fitting the permittivity calibration curves (Figure 9) can account for the corresponding low R^2 values obtained for the calibration surfaces. Thus, the permittivity surfaces were modeled in

accordance with Eq. 4 using a polynomial of degree 2 with respect to the y-axis in order to yield a coefficient regression R^2 equal to 0.97.

$$\text{Log}\ (\rho\ (\text{Ohm.m})) = a + b.\ C + c.\ S_r \qquad \text{Eq. 3}$$

$$\varepsilon\ (-) = a + b.\ C + c.\ S_r + d.\ S_r.\ C + e.\ S_r^{\,2} \qquad \text{Eq. 4}$$

The resistivity and permittivity calibration surfaces are presented in Figure 10 and Figure 11 for both concretes, respectively. Only the calibration surfaces relative to **total** chloride content are actually presented. Indeed, the concentration of the free chloride ions located in the pore solution depends on the water content as well as on the degree of saturation. The free chloride concentration determined by DE after the last targeted degree of saturation in fact does not represent the 'real' free chloride concentration determined for the other degrees of saturation. Thus, only the calibration surfaces derived from the total chloride concentration are presented in this paper. Nevertheless, the coefficients of the calibration surface equation have been determined for both the 'free' and 'total' chloride concentrations and are presented in this paper. The coefficients of the resistivity and permittivity calibration equations are listed in Table 3 and Table 4, respectively.

Moreover, let's note the very small difference between the coefficients obtained through using the free and total chloride concentrations. As seen in Figure 8 or Figure 9, the free and total chloride concentrations are quite similar, which could explain the small difference between the equation coefficients for both concretes.

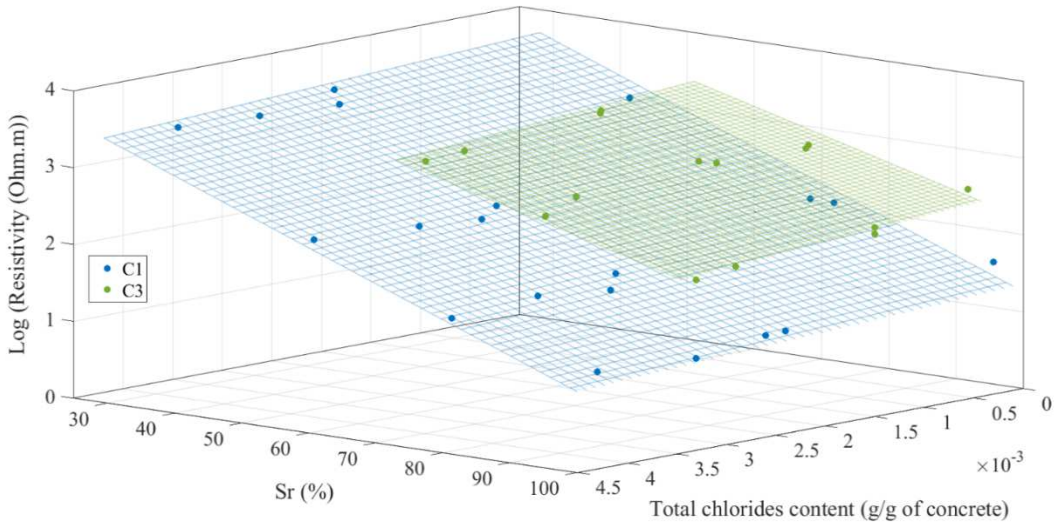

Figure 10: Resistivity surface based on total chloride content and degree of saturation for concretes C1 (blue) and C3 (green)

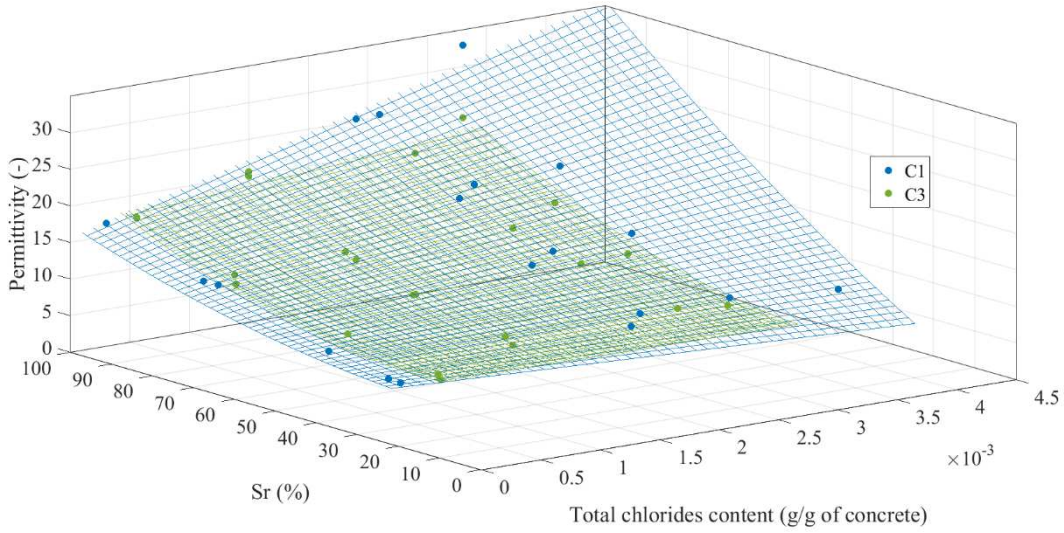

Figure 11: Permittivity surface based on total chloride content and degree of saturation for concretes C1 (blue) and C3 (green)

Table 3: Coefficients of the **resistivity** calibration surface equation as a function of the free and total chloride contents and degree of saturation

	a	b	c	R^2	RMSE
C1-Free chlorides	4.69	-61.27	-0.0338	0.92	0.2487
C1-Total chlorides	4.75	-69.48	-0.0033	0.92	0.2418
C3-Free chlorides	4.90	-101.5	-0.0235	0.96	0.0855
C3-Total chlorides	4.94	-97.43	-0.0236	0.95	0.0877

Table 4: Coefficients of the **permittivity** calibration surface equation as a function of the free and total chloride contents and degree of saturation

	a	b	c	d	e	R^2	RMSE
C1-Free chlorides	6.53	-2974	-0.0077	81.49	0.0011	0.97	1.247
C1-Total chlorides	6.72	-2412	-0.0172	68.75	0.0010	0.98	0.9743
C3-Free chlorides	8.70	-588.4	-0.1024	18.75	0.0019	0.97	0.8953
C3-Total chlorides	8.80	-544	-0.1063	17.73	0.0019	0.97	0.9004

3.3. Leveraging of calibration surfaces

The novelty of this work lies in the comprehensive and systematic exploration of these calibration surfaces, thus highlighting the intricate interplay between the resistivity and permittivity of concrete with varying chloride and water contents. Previous studies have not offered such an exploratory approach.

Nevertheless, the EM properties of concrete are known to vary depending on factors such as the binder (supplementary cementitious materials effects), water-to-binder ratio and aggregate type to name just a few. Therefore, it is crucial to consider these calibration surfaces as intrinsic properties unique to the concrete mixtures C1 and C3 investigated in this study. For other mixtures with different compositions, it would be necessary to repeat the calibration process in order to establish accurate and specific calibration surfaces. The insights gained from this study regarding the methodology and approach to calibration can still provide valuable guidance for future research on other concrete mixtures. Depending on the degree of polynomial obtained for the equations representing the resistivity and permittivity surfaces, it will be possible to establish calibration surfaces by using only two sodium chloride concentrations within the range of 0 to 90 g/L and considering only three different levels of saturation.

Moreover, to effectively measure the resistivity of high-resistivity concrete such as concrete C3, it is advisable to consider a range of degrees of saturation lying between 100% and 60%. This approach is justified due to the infeasibility of measurements at lower degrees of saturation for this type of high concrete resistivity, as was it is recommended to avoid degrees of saturation below 35% for ordinary concretes, e.g. C1. This selection of parameters offers substantial potential for minimizing the time and workload associated with such investigations.

Regarding the degrees of saturation of the concrete cores, it is advisable to determine the porosity of each individual core rather than relying solely on the overall porosity of the concrete obtained from just three different samples. This step can be accomplished by keeping one sawn portion of each core (as illustrated in Step 1 of Figure 3) and then determining its porosity by means of hydrostatic weighing. The remaining two portions will be utilized for determining the chloride content. By adopting this approach, the reliability of the obtained degree of saturation measurements is enhanced.

Lastly, it is crucial to determine the concentration of free chlorides at each degree of saturation reached. This step is essential for obtaining an accurate measurement of the free chloride concentration, thus enabling more reliable assessments and evaluations.

4. Conclusion

This paper has presented a novel calibration approach aimed at determining the calibration curves and the calibration surfaces of electromagnetic (EM) parameters, specifically concrete resistivity and permittivity, by simultaneously considering the water and chloride contents of concrete. The investigation has focused on two concrete mixtures to assess the impact of incorporating slag on these parameters.

The results have led to the following conclusions:

- The dielectric permittivity exhibited ascending calibration curves and calibration surfaces as water and chloride contents increased. In contrast, the electrical resistivity displayed descending surfaces and curves.
- The concrete resistivity displayed a high sensitivity to saturation rather than to the chloride concentration, with infeasible resistivity measurements at low degrees of saturation, especially for concrete C3.
- The presence of slag in the concrete has no remarkable effect on permittivity, with identical values found for both concretes at different degrees of saturation without chloride.
- The concrete permittivity evolution relative to different chloride contents did not reveal the same trend, with a higher sensitivity for concrete C1. The slope of the calibration curve is approximately three times greater for concrete C1 than that obtained for concrete C3.
- The use of logarithmic resistivity values led to removing the quadratic effect and obtaining a surface with a polynomial equation of degree one with respect to both the x-axis and y-axis.
- The polynomial degree derived for the calibration surface equations of both concrete mixtures serves as a crucial tool for establishing new calibration surfaces for other concrete mixtures.
- The calibration surfaces versus total chloride content were solely presented in this work since the free chloride content depends on the degree of saturation. In future work, the experimental protocol should be modified by determining both the free and

total content at each degree of saturation, so as to determine the calibration surface with a lower uncertainty.

In future studies, the calibration surfaces will be used as a valuable tool, when dealing with a coupled water-chloride ingress test, in converting the dielectric permittivity and electrical resistivity profiles into chloride and degree of saturation profiles. Also, these profiles will be used to determine additional durability indicators such as the apparent diffusion coefficient, the surface chloride concentration or water permeability by inverse analysis according to water-chloride ingress models.

5. Acknowledgements

The authors would like to thank the MAST-LAMES Laboratory at the Université Gustave Eiffel and the GeM Laboratory at Nantes University for their financial contribution to the experimental campaign.

6. References

[1] S. Feliu, C. Andrade, J.A. González, C. Alonso, A new method fori n-situ measurement of electrical resistivity of reinforced concrete, Mat. Struct. 29 (1996) 362–365. https://doi.org/10.1007/BF02486344.

[2] C.E.T. Balestra, T.A. Reichert, W.A. Pansera, G. Savaris, Evaluation of chloride ion penetration through concrete surface electrical resistivity of field naturally degraded structures present in marine environment, Construction and Building Materials. 230 (2020) 116979. https://doi.org/10.1016/j.conbuildmat.2019.116979.

[3] C.E.T. Balestra, A.Y. Nakano, G. Savaris, R.A. Medeiros-Junior, Reinforcement corrosion risk of marine concrete structures evaluated through electrical resistivity: Proposal of parameters based on field structures, Ocean Engineering. 187 (2019) 106167. https://doi.org/10.1016/j.oceaneng.2019.106167.

[4] G. Villain, Z.M. Sbartaï, X. Dérobert, V. Garnier, J.P. Balayssac, Durability diagnosis of a concrete structure in a tidal zone by combining NDT methods: Laboratory tests and case study, Construction and Building Materials. 37 (2012) 893–903. https://doi.org/10.1016/j.conbuildmat.2012.03.014.

[5] X. Dérobert, J.-P. Balayssac, Z.M. Sbartaï, J. Dumoulin, Chapter 3 - Electromagnetic Methods, in: J.-P. Balayssac, V. Garnier (Eds.), Non-Destructive Testing and Evaluation of Civil Engineering Structures, Elsevier, 2018: pp. 87–137. https://doi.org/10.1016/B978-1-78548-229-8.50003-0.

[6] G. Villain, A. Ihamouten, R. du Plooy, S.P. Lopes, X. Dérobert, Use of electromagnetic non-destructive techniques for monitoring water and chloride ingress into concrete, Near Surface Geophysics. 13 (2015) 299–309. https://doi.org/10.3997/1873-0604.2015016.

[7] R.A. Medeiros-Junior, M.G. Lima, Electrical resistivity of unsaturated concrete using different types of cement, Construction and Building Materials. 107 (2016) 11–16. https://doi.org/10.1016/j.conbuildmat.2015.12.168.

[8] J. Priou, Y. Lecieux, M. Chevreuil, V. Gaillard, C. Lupi, D. Leduc, E. Rozière, R. Guyard, F. Schoefs, In situ DC electrical resistivity mapping performed in a reinforced concrete wharf using embedded sensors, Construction and Building Materials. 211 (2019) 244–260. https://doi.org/10.1016/j.conbuildmat.2019.03.152.

[9] D. Lim, S. Teng, B. Sabet Divsholi, O. Gjørv, Durability of Very-High-Strength Concrete with Supplementary Cementitious Materials for Marine Environments, ACI Materials Journal. 113 (2016). https://doi.org/10.14359/51687981.

[10] J.-F. Lataste, G. Villain, J.-P. Balayssac, Chapter 4 - Electrical Methods, in: J.-P. Balayssac, V. Garnier (Eds.), Non-Destructive Testing and Evaluation of Civil Engineering Structures, Elsevier, 2018: pp. 139–172. https://doi.org/10.1016/B978-1-78548-229-8.50004-2.

[11] M.K. EL Achrafi, S. Bonnet, G. Villain, Electrical resistivity tomography results analyzed with two inversion methods to determine chloride profiles on BFS concrete having very high electrical resistivity, Construction and Building Materials. 407 (2023) 133361. https://doi.org/10.1016/j.conbuildmat.2023.133361.

[12] F. Hunkeler, The resistivity of pore water solution—a decisive parameter of rebar corrosion and repair methods, Construction and Building Materials. 10 (1996) 381–389. https://doi.org/10.1016/0950-0618(95)00029-1.

[13] Z.M. Sbartaï, S. Laurens, J. Rhazi, J.P. Balayssac, G. Arliguie, Using radar direct wave for concrete condition assessment: Correlation with electrical resistivity, Journal of Applied Geophysics. 4 (2007) 361–374. https://doi.org/10.1016/j.jappgeo.2007.02.003.

[14] R.B. Polder, Test methods for on site measurement of resistivity of concrete - a RILEM TC-154 technical recommendation, 15 (2001) 125–131.

[15] R.L. Henry, Water vapour transmission and electrical resistivity of concrete, US Naval Civil Engineering Laboratory, Port Hueneme, California, USA. (1964).

[16] G.E. Archie, The Electrical Resistivity Log as an Aid in Determining Some Reservoir Characteristics, Transactions of the AIME. 146 (1942) 54–62. https://doi.org/10.2118/942054-G.

[17] T. Hanai, Theory of the dielectric dispersion due to the interfacial polarization and its application to emulsions, Kolloid-Zeitschrift. 171 (1960) 23–31. https://doi.org/10.1007/BF01520320.

[18] X. Dérobert, G. Villain, R. Cortas, J.L. Chazelas, EM characterization of hydraulic concretes in the GPR frequency-band using a quadratic experimental design, E-Journal of Nondestructive Testing. 14 (7) (2009).

[19] S. Laurens, J.-P. Balayssac, J. Rhazi, G. Arliguie, Influence of concrete relative humidity on the amplitude of Ground-Penetrating radar (GPR) signal, Mat. Struct. 35 (2002) 198–203. https://doi.org/10.1007/BF02533080.

[20] T. Fen-Chong, A. Fabbri, J.-P. Guilbaud, O. Coussy, Determination of liquid water content and dielectric constant in porous media by the capacitive method, Comptes Rendus de l'Académie Des Sciences. Série IIb, Mécanique. 332 (2004) 639. https://doi.org/10.1016/j.crme.2004.02.028.

[21] R. du Plooy, G. Villain, S. Palma Lopes, A. Ihamouten, X. Dérobert, B. Thauvin, Electromagnetic non-destructive evaluation techniques for the monitoring of water and

chloride ingress into concrete: a comparative study, Mater Struct. 48 (2015) 369–386. https://doi.org/10.1617/s11527-013-0189-z.

[22] D.J. Daniels, Ground Penetrating Radar., 2nd Edition, IEE Radar, Sonar and Navigation Series 15, The Institution of Electrical Engineers, London., n.d.

[23] Y. Abbas, F. Pargar, D.A. Koleva, K. van Breugel, W. Olthuis, A. van den Berg, Non-destructive measurement of chloride ions concentration in concrete – A comparative analysis of limitations and prospects, Construction and Building Materials. 174 (2018) 376–387. https://doi.org/10.1016/j.conbuildmat.2018.04.135.

[24] O. Poupard, A. Aït-Mokhtar, P. Dumargue, Corrosion by chlorides in reinforced concrete: Determination of chloride concentration threshold by impedance spectroscopy, Cement and Concrete Research. 34 (2004) 991–1000. https://doi.org/10.1016/j.cemconres.2003.11.009.

[25] W.J. McCarter, M.C. Forde, H.W. Whittington, Resistivity characterstics of concrete, Proc. Instn Civ. Engrs. 71 (1981) 107–117.

[26] R. Spragg, J. Castro, T. Nantung, M. Paredes, W. Weiss, Variability Analysis of the Bulk Resistivity Measured Using Concrete Cylinders, JTRP Technical Reports. (2011). https://doi.org/10.5703/1288284314646.

[27] D. Smyl, Relating unsaturated electrical and hydraulic conductivity of cement-based materials, Australian Journal of Civil Engineering. 16 (2018). https://doi.org/10.1080/14488353.2018.1473832.

[28] G. Villain, V. Garnier, Z.M. Sbartaï, X. Dérobert, J.P. Balayssac, Development of a calibration methodology to improve the on-site non-destructive evaluation of concrete durability indicators, Mater Struct. 51 (2018) 40. https://doi.org/10.1617/s11527-018-1165-4.

[29] J. Badr, Y. Fargier, S. Palma-Lopes, F. Deby, J. Balayssac, S. Delepine-Lesoille, L.-M. Cottineau, G. Villain, Design and validation of a multi-electrode embedded sensor to monitor resistivity profiles over depth in concrete, Construction and Building Materials. 223 (2019) 310–321. https://doi.org/10.1016/j.conbuildmat.2019.06.226.

[30] M.A. Alhajj, S. Bourguignon, S. Palma Lopes, G. Villain, Joint inversion of electromagnetic measurements for the determination of water saturation profiles in concrete structures, Cement and Concrete Research. 147 (2021) 106500. https://doi.org/10.1016/j.cemconres.2021.106500.

[31] M. Fares, G. Villain, S. Bonnet, S. Palma Lopes, B. Thauvin, M. Thiery, Determining chloride content profiles in concrete using an electrical resistivity tomography device, Cement and Concrete Composites. 94 (2018) 315–326. https://doi.org/10.1016/j.cemconcomp.2018.08.001.

[32] M. Fares, Y. Fargier, G. Villain, X. Derobert, S. Palma Lopes, Determining the permittivity profile inside reinforced concrete using capacitive probes, NDT & E International. 79 (2016) 150–161. https://doi.org/10.1016/j.ndteint.2016.01.002.

[33] G. Klysz, J.P. Balayssac, Determination of volumetric water content of concrete using ground-penetrating radar, Cement and Concrete Research. 37 (2007) 1164–1171. https://doi.org/10.1016/j.cemconres.2007.04.010.

[34] W. Chen, P. Shen, Z. Shui, Determination of water content in fresh concrete mix based on relative dielectric constant measurement, Construction and Building Materials. 34 (2012) 306–312. https://doi.org/10.1016/j.conbuildmat.2012.02.073.

[35] R. Sriravindrarajah, R. Swamy, Development of a Conductivity Probe to Monitor Setting Time and Moisture Movement in Concrete, Cement, Concrete, Aggr. 4 (1982) 73. https://doi.org/10.1520/CCA10231J.

[36] S. Bonnet, J.-P. Balayssac, Combination of the Wenner resistivimeter and Torrent permeameter methods for assessing carbonation depth and saturation level of concrete, Construction and Building Materials. 188 (2018) 1149–1165. https://doi.org/10.1016/j.conbuildmat.2018.07.151.

[37] M. Saleem, M. Shameem, S.E. Hussain, M. Maslehuddin, Effect of moisture, chloride and sulphate contamination on the electrical resistivity of Portland cement concrete, Construction and Building Materials. 10 (1996) 209–214. https://doi.org/10.1016/0950-0618(95)00078-X.

[38] Y. Lecieux, F. Schoefs, S. Bonnet, T. Lecieux, S. Palma Lopes, Quantification and uncertainty analysis of a structural monitoring device: detection of chloride in concrete using DC electrical resistivity measurement, Nondestructive Testing and Evaluation. 30 (2015) 216–232. https://doi.org/10.1080/10589759.2015.1029476.

[39] G.R. Meira, C. Andrade, I.J. Padaratz, C. Alonso, J.C. Borba, Chloride penetration into concrete structures in the marine atmosphere zone – Relationship between deposition of chlorides on the wet candle and chlorides accumulated into concrete, Cement and Concrete Composites. 29 (2007) 667–676. https://doi.org/10.1016/j.cemconcomp.2007.05.009.

[40] C.E.T. Balestra, T.A. Reichert, W.A. Pansera, G. Savaris, Chloride profile modeling contemplating the convection zone based on concrete structures present for more than 40 years in different marine aggressive zones, Construction and Building Materials. 198 (2019) 345–358. https://doi.org/10.1016/j.conbuildmat.2018.11.271.

[41] T. Luping, Resistance of Concrete to Chloride Ingress: Testing and modelling, CRC Press, Taylor & Francis Group. (2013) 264. https://doi.org/10.1201/b12603.

[42] R. Cai, Y. Hu, M. Yu, W. Liao, L. Yang, A. Kumar, H. Ma, Skin effect of chloride ingress in marine concrete: A review on the convection zone, Construction and Building Materials. 262 (2020) 120566. https://doi.org/10.1016/j.conbuildmat.2020.120566.

[43] ASTM C989-05, Standard Specification for Ground Granulated Blast-Furnace Slag for Use in Concrete and Mortars, (2005).

[44] CEN. (2004), EN 206-1 Concrete - Part 1: Specification, performances, production and conformity., (n.d.).

[45] CEN. (2005), EN 1992-1-1 Eurocode 2 - Design of concrete structure - Part 1.1 General rules and rules for buildings. European Standard Organization., (n.d.).

[46] G. Arliguie, H. Hornain, GranDuBé – Grandeurs associées à la durabilité des bétons (durability-related parameters_in French), RGCU–AFGC–Presses de l'ENPC, Paris. (2007) 63–106.

[47] R. Du Plooy, S. Palma Lopes, G. Villain, X. Dérobert, Development of a multi-ring resistivity cell and multi-electrode resistivity probe for investigation of cover concrete

condition, NDT & E International. 54 (2013) 27–36. https://doi.org/10.1016/j.ndteint.2012.11.007.

[48] M. Adous, P. Quéffélec, L. Laguerre, Coaxial/cylindrical transition line for broadband permittivity measurement of civil engineering materials, Meas. Sci. Technol. 17 (2006) 2241–2246. https://doi.org/10.1088/0957-0233/17/8/026.

[49] A. Robert, Dielectric permittivity of concrete between 50 Mhz and 1 Ghz and GPR measurements for building materials evaluation, Journal of Applied Geophysics. 40 (1998) 89–94. https://doi.org/10.1016/S0926-9851(98)00009-3.

[50] R.T. 178-TMC, Recommendations of RILEM TC 178-TMC : "Testing and modelling chloride penetration in concrete" Analysis of water soluble chloride content in concrete, Materials and Structures. 35 (2002) 586–588.

[51] R.T. 178-TMC, Recommendations of RILEM TC 178-TMC : "Testing and modelling chloride penetration in concrete" Analysis of total chloride content in concrete, 35 (2002) 583–585.

[52] K. Ito, T. Hirokawa, Chapter 9 - Iodine and Iodine Species in Seawater: Speciation, Distribution, and Dynamics, in: V.R. Preedy, G.N. Burrow, R. Watson (Eds.), Comprehensive Handbook of Iodine, Academic Press, San Diego, 2009: pp. 83–91. https://doi.org/10.1016/B978-0-12-374135-6.00009-1.

[53] C. Arya, N.R. Buenfeld, J.B. Newman, Factors influencing chloride-binding in concrete, Cement and Concrete Research. 20 (1990) 291–300. https://doi.org/10.1016/0008-8846(90)90083-A.

[54] A. Djerbi, Influence de l'endommagement mécanique sur la perméabilité au gaz et sur la diffusion des ions chlorure des bétons, Thèse de doctorat, Université de Nantes, 2007.

[55] L.J. Parrott, Moisture conditioning and transport properties of concrete test specimens, Materials and Structures. 27 (1994) 460. https://doi.org/10.1007/BF02473450.

[56] M.H. Loke, Tutorial : 2-D and 3-D electrical imaging surveys, (2015) 187.

[57] H.K. Johansen, A man/computer interpretation system for resistivity soundings over a horizontally strafified earth, Geophysical Prospecting. 25 (1977) 667–691. https://doi.org//10.1111/j.1365-2478.1977.tb01196.x.

[58] K. Hornbostel, C.K. Larsen, M.R. Geiker, Relationship between concrete resistivity and corrosion rate – A literature review, Cement and Concrete Composites. 39 (2013) 60–72. https://doi.org/10.1016/j.cemconcomp.2013.03.019.

[59] A. Lübeck, A.L.G. Gastaldini, D.S. Barin, H.C. Siqueira, Compressive strength and electrical properties of concrete with white Portland cement and blast-furnace slag, Cement and Concrete Composites. 34 (2012) 392–399. https://doi.org/10.1016/j.cemconcomp.2011.11.017.

[60] A. Darquennes, S. Staquet, A. Kamen, M. Delplancke, B. Espion, Early age properties development of concrete with different slag contents, American Concrete Institute, ACI Special Publication. (2009) 35–57.

[61] A. Darquennes, B. Espion, S. Staquet, How to assess the hydration of slag cement concretes?, Construction and Building Materials. 40 (2013) 1012–1020. https://doi.org/10.1016/j.conbuildmat.2012.09.087.

[62] İ. Yüksel, T. Bilir, Ö. Özkan, Durability of concrete incorporating non-ground blast furnace slag and bottom ash as fine aggregate, Building and Environment. 42 (2007) 2651–2659. https://doi.org/10.1016/j.buildenv.2006.07.003.

[63] B.S. Divsholi, L. Lim T.Y.D., S. Teng, Durability Properties and Microstructure of Ground Granulated Blast Furnace Slag Cement Concrete, Int J Concr Struct Mater. 8 (2014) 157–164. https://doi.org/10.1007/s40069-013-0063-y.

[64] A. Elahi, P.A.M. Basheer, S.V. Nanukuttan, Q.U.Z. Khan, Mechanical and durability properties of high performance concretes containing supplementary cementitious materials, Construction and Building Materials. 24 (2010) 292–299. https://doi.org/10.1016/j.conbuildmat.2009.08.045.

[65] Y. Guéguen, V. Palciauskas, Introduction à la physique des roches, Hermann Paris, 1992.

[66] V. Baroghel-Bouny, K. Kinomura, M. Thiery, S. Moscardelli, Easy assessment of durability indicators for service life prediction or quality control of concretes with high volumes of supplementary cementitious materials, Cement and Concrete Composites. 33 (2011) 832–847. https://doi.org/10.1016/j.cemconcomp.2011.04.007.